OPEN ACCESS
CellPress

Cell Reports
Report

In Vitro-Reconstituted Nucleoids Can Block Mitochondrial DNA Replication and Transcription

Géraldine Farge,[1,4] Majda Mehmedovic,[2,4] Marian Baclayon,[1] Siet M.J.L. van den Wildenberg,[3] Wouter H. Roos,[1] Claes M. Gustafsson,[2] Gijs J.L. Wuite,[1,5,*] and Maria Falkenberg[2,5,*]
[1]Department of Physics and Astronomy and LaserLaB, VU University, De Boelelaan 1081, 1081 HV Amsterdam, the Netherlands
[2]Department of Medical Biochemistry and Cell Biology, University of Gothenburg, P.O. Box 440, SE-405 30 Gothenburg, Sweden
[3]Institut Langevin, ESPCI ParisTech, 1, rue Jussieu, 75238 Paris Cedex 05, France
[4]Co-first author
[5]Co-senior author
*Correspondence: g.j.l.wuite@vu.nl (G.J.L.W.), maria.falkenberg@medkem.gu.se (M.F.)
http://dx.doi.org/10.1016/j.celrep.2014.05.046

SUMMARY

The mechanisms regulating the number of active copies of mtDNA are still unclear. A mammalian cell typically contains 1,000–10,000 copies of mtDNA, which are packaged into nucleoprotein complexes termed nucleoids. The main protein component of these structures is mitochondrial transcription factor A (TFAM). Here, we reconstitute nucleoid-like particles in vitro and demonstrate that small changes in TFAM levels dramatically impact the fraction of DNA molecules available for transcription and DNA replication. Compaction by TFAM is highly cooperative, and at physiological ratios of TFAM to DNA, there are large variations in compaction, from fully compacted nucleoids to naked DNA. In compacted nucleoids, TFAM forms stable protein filaments on DNA that block melting and prevent progression of the replication and transcription machineries. Based on our observations, we suggest that small variations in the TFAM-to-mtDNA ratio may be used to regulate mitochondrial gene transcription and DNA replication.

INTRODUCTION

A mammalian cell contains multiple copies of mtDNA, a circular molecule of 16,569 bp that encodes for 13 essential subunits of the respiratory chain. The genome is essential for normal cellular function; mtDNA mutations can cause mitochondrial disease and have also been implicated in human aging (Park and Larsson, 2011). In vivo, mtDNA exists in a compact nucleoprotein complex, denoted the nucleoid (Bogenhagen, 2012). Most nucleoids contain a single mtDNA molecule, which is fully coated by mitochondrial transcription factor A (TFAM), a high-mobility-group box domain protein (Brown et al., 2011; Kukat et al., 2011; Wang et al., 2013). In vivo estimates have determined the concentration of TFAM to one molecule per 15 to 18 bp of mtDNA (Kukat et al., 2011), and TFAM is to date the only protein shown to package and organize mtDNA. Volume calculations suggest that TFAM is the major constituent of the nucleoid, even if other proteins, such as mtDNA replication and transcription factors, can associate with this structure (Kukat and Larsson, 2013). TFAM binds in a cooperative manner to nonspecific DNA sequences and forms stable protein patches (filaments) in which each monomer covers about 30 bp of DNA. TFAM binding leads to partial unwinding of duplex DNA, which in turn causes softening and compaction of the DNA molecule (Farge et al., 2012).

TFAM is essential for mtDNA maintenance. Disruption of the *Tfam* gene in mouse causes loss of mtDNA, whereas overexpression of TFAM leads to increased mtDNA copy number (Ekstrand et al., 2004; Kanki et al., 2004; Larsson et al., 1998). TFAM is also an essential component of the mtDNA transcription machinery (Shi et al., 2012). The protein binds in a sequence-specific manner to mitochondrial promoters and induces a stable U-turn in DNA (Ngo et al., 2011; Rubio-Cosials et al., 2011). In combination with mitochondrial RNA polymerase (POLRMT) and the mitochondrial transcription factor B2 (TFB2M), TFAM supports transcription from the mitochondrial heavy- and light-strand promoters (HSP and LSP) in vitro (Falkenberg et al., 2002; Fisher and Clayton, 1985). Mammalian mitochondria also contain specialized DNA replication machinery, which includes DNA polymerase γ (POLγ), the replicative helicase TWINKLE, and mitochondrial single-stranded DNA-binding protein (mtSSB). When combined, these factors can support leading-strand DNA synthesis in vitro (Korhonen et al., 2004).

In the nucleus, DNA compaction by histones into nucleosomes negatively regulates DNA transactions, such as DNA replication and transcription (Finkelstein and Greene, 2013). TFAM-dependent compaction of mtDNA will most likely also have consequences for the activity of DNA-binding molecular machines. Here, we elucidate how the moving replication and transcription machineries react to roadblocks formed by TFAM using a combination of classical biochemical techniques and single-molecule tools. We provide evidence that high TFAM:mtDNA ratios result in the formation of large stable TFAM filaments on the DNA that reduce the progression of replication and transcription complexes. Moreover, we show that at in vivo-relevant concentrations of TFAM, there is a large variation in the amount of compaction among different DNA molecules. At these conditions, small changes in the TFAM concentration have a large impact on the average compaction, as would be expected if TFAM is used as a global regulator for mtDNA transactions.

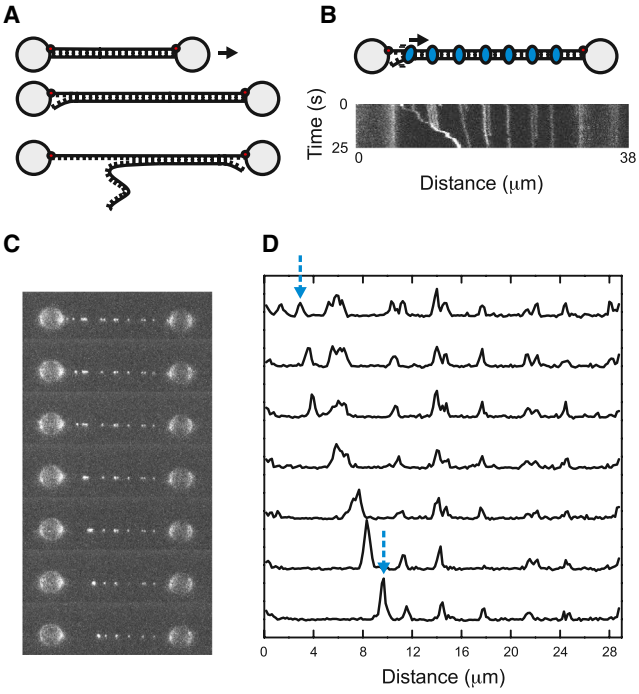

Figure 1. TFAM Is Pushed on DNA during Peeling

(A) The force-induced DNA-peeling strategy. Optically trapped beads are represented in gray, and biotin-streptavidin linkages between the DNA molecule and the trapped beads are depicted in red.

(B) Schematic depiction of DNA covered with TFAM (in blue) undergoing peeling. Kymograph generated from the successive frames of a movie (Movie S1) showing TFAM molecules being pushed on dsDNA. Time (s) and distance (μm) are indicated at the left and bottom, respectively.

(C) Selected frames (time interval 3 s) from a movie showing the behavior of fluorescent TFAM on a DNA molecule that is undergoing peeling while kept at a constant tension (65 pN; relative DNA extension L/Lc = 1.6).

(D) Intensity plot (fluorescence intensity as a function of time) of the frames shown in (C). The blue arrows show the increase of intensity of the moving fluorescent spot.

Both the kymograph represented in (B) and the selected frames depicted in (C) were obtained from Movie S1.

RESULTS

TFAM Is Pushed Forward on Double-Stranded DNA during Strand Separation

The elongation stages of mtDNA replication and transcription require that the double-stranded DNA (dsDNA) template is partially unwound. We developed a single-molecule assay in which force-induced melting/peeling of dsDNA mimicked strand invasion by a motor protein and monitored the effect TFAM packaging may have on this process (Figure 1A). A dsDNA molecule (lambda DNA ~48 kbp) was labeled with biotin on both the 5′ and 3′ ends of the same strand and attached between two beads held in a dual optical trap. The DNA molecule was then progressively extended ~75% into its overstretching plateau (65 pN) and held under this tension during the experiment. Due to both the labeling strategy (the dsDNA molecule has two free ends) and the salt concentration used in this assay (25 mM NaCl), the overstretching of a dsDNA molecule results in base-pair breaking from the free DNA ends that leads to a progressive conversion of the dsDNA into two single-stranded DNA (ssDNA) strands, with only the strand with the biotins still under tension (Candelli et al., 2013; King et al., 2013). To monitor what happens to TFAM during DNA strand separation, we incubated the relaxed DNA construct with fluorescently labeled TFAM (Alexa555), overstretched the DNA into the overstretching plateau, and excited the Alexa555 in a continuous fashion while detecting the emitted fluorescence. We first checked the impact of high force on the TFAM-DNA interactions and found that, in the overstretching regime, the dissociation time of TFAM from DNA was not significantly different from those observed previously for forces up to 40 pN (Farge et al., 2012). When keeping the DNA 75% overstretched, we observed a unidirectional displacement of some TFAM molecules along the DNA contour (Figures 1B–1D; Movie S1). We observed this pattern repeatedly and we monitored in total more than 200 fluorescent spots on the DNA. We could also observe a progressive increase of fluorescent intensity as a moving fluorescent spot encountered other stationary fluorescent proteins (Figure 1D, blue arrow). We hypothesized that these events are the result of TFAM molecules being progressively pushed by the junction between the ssDNA and dsDNA during strand separation. To confirm this hypothesis, we needed to follow the peeling process directly, by localizing the single-stranded and double-stranded regions of the DNA molecule. To this end, we performed experiments similar to the one presented in Figure 1 but in the presence of replication protein A (RPA), which binds selectively to ssDNA (King et al., 2013; van Mameren et al., 2009). We first incubated the relaxed dsDNA molecule in a channel containing fluorescent TFAM. We then transferred the DNA molecule into a buffer containing RPA fluorescently labeled with enhanced GFP (eGFP-RPA) and overstretched the DNA to ~70%. Finally, we excited alternatively with appropriate light to image RPA and TFAM and to obtain an overlay of the two images (Figure 2A). We found that eGFP-RPA binds preferentially to the extremities of the DNA where the strand separation starts, indicating that this part is single stranded. We noticed that eGFP-RPA also binds, but to a lesser extent, to the middle region of the DNA. Under low-ionic-strength conditions and upon extension of a DNA molecule far into its overstretching plateau, we have previously observed scattered RPA binding all through the DNA molecule. This is explained by the presence of RPA (and thus ssDNA) at localized domains where base-pairing is broken (so-called melting bubbles) and the phosphate backbones remain under tension (King et al., 2013). At the same time, we observed that most TFAM binding does not overlap with RPA binding. Due to the optical resolution limit (diffraction limit ~300 nm), we cannot spatially separate RPA and TFAM binding when they are bound closer than ~750 bps to one another, but the majority of TFAM could unequivocally be assigned to the double-stranded region of the DNA construct. When we extended the DNA molecule far into the overstretching plateau (~85%), we observed eGFP-RPA binding throughout the whole DNA molecule consistent with the formation of melting bubbles (Figure 2B). The presence of melting bubbles explains why one can observe a "thicker" red line in the middle of the DNA molecule compared to its left side; in a melting bubble (middle of the molecule), the two strands are

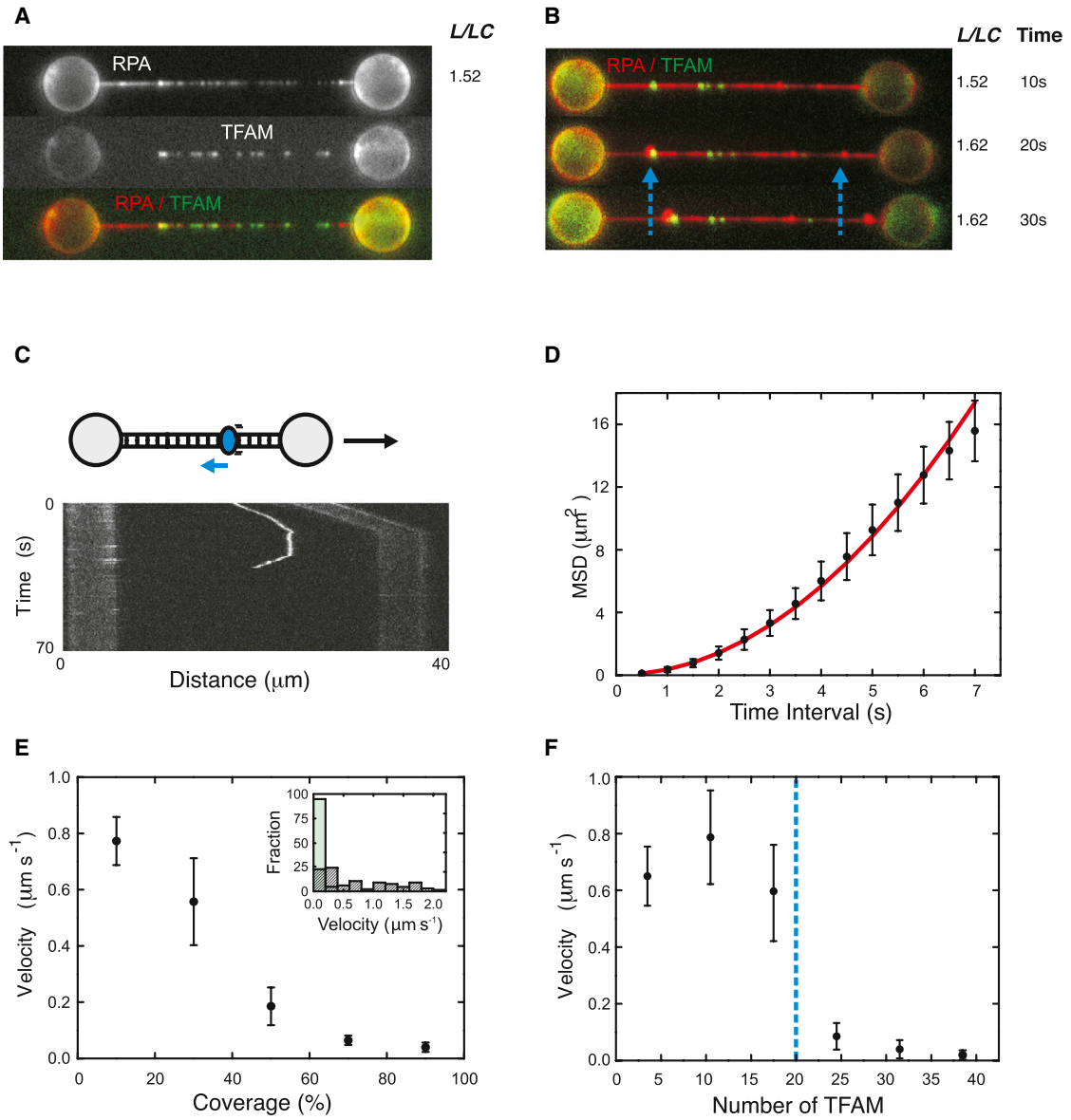

Figure 2. TFAM Localizes on the dsDNA at the Melting Front and Can Prevent Peeling

(A) Fluorescence images of eGFP-RPA and Alexa555-TFAM and composite fluorescence images displaying the binding of eGFP-RPA (in red) and Alexa555-TFAM (in green).

(B) Selection of fluorescence images (time interval 10 s) showing the binding of eGFP-RPA (in red) and Alexa555-TFAM (in green). The arrows indicate the peeling events. For both panels, the dsDNA molecules were incubated with Alexa555-TFAM (20 nM), overstretched, and incubated with eGFP-RPA (2 nM). The relative DNA extension (*L*/*Lc*) is indicated in the figure.

(C) Kymograph showing a TFAM patch (fluorescence intensity corresponds to four TFAM molecules) moving on a DNA molecule undergoing peeling.

(D) The position of the moving patch showed in (C) was tracked and the mean square displacement (MSD) was determined. The MSD plot was fitted (MSD = v^2t^2 + 2Dt) to determine the velocity (v) of the molecule and the diffusion coefficient (D) (t is time).

(E) The obtained velocities for the observed TFAM molecules (n = 221) were binned into five equal-sized bins according to the fraction of TFAM coverage on the DNA. The percentage coverage was calculated using the DNA persistence length (obtained by fitting the DNA force extension curves with the worm like chain model) as described in Farge et al. (2012). Inset: histogram of the distribution of the observed velocities at high TFAM coverage (≥50%, light green bars) and low TFAM coverage (<50%, crossed bars).

(F) The velocities at low TFAM coverage (<10%) (n = 53) were binned into five equal-sized bins according to the number of TFAM in a spot and plotted as a function of number of TFAM. The number of TFAMs in each fluorescent spot was determined by single photobleaching steps.

See also Figure S1.

RPA coated, which results in a higher RPA concentration compared to a peeled ssDNA molecule being coated by RPA (left side of the molecule). However, at the ionic strength conditions used, peeling from the extremities is energetically favorable over the formation of melting bubbles (King et al., 2013). Indeed, when we kept the DNA overstretched and imaged the DNA, we could observe that peeling actually progresses on the DNA molecule, albeit rather slow (Figure 2B, the blue arrows show two peeling fronts, one starting on the left from the extremity of the DNA and one from a nick in the DNA on the right). As expected, the slow peeling (left side) is correlated with a TFAM patch localized in the double-stranded region of the DNA molecule that impedes the peeling process. Note also that TFAM is not present in the DNA strand that is free (bulge next to the left blue arrow), staying exclusively on the DNA that is not peeled off. We thus conclude that TFAM moves in a unidirectional way along the dsDNA during DNA peeling. We observed similar patterns several times; however, to obtain quantitative data of the pushing of TFAM on DNA by ssDNA peeling, we chose to use naked DNA molecules to completely exclude possible interferences between RPA and either the unpeeling process or the binding of TFAM on DNA.

High TFAM Coverage of the DNA Prevents DNA Strand Separation

We next characterized the movement of TFAM during DNA strand separation as a function of protein concentration. For each fluorescent spot on the DNA (like those on Figure 2C or Figure 1), we recorded a movie and tracked the (possible) movement of TFAM molecules on the DNA undergoing peeling by fitting a 2D Gaussian to the intensity profile in each frame. From the trajectories obtained, we calculated the mean square displacement and fitted it as a function of the time interval (Figure 2D). Under normal conditions, TFAM diffuses or remains stationary on DNA (the later is typically seen at high TFAM concentrations). When DNA is undergoing peeling, we could observe TFAM moving directionally, indicating that strand separation is pushing the TFAM forward. We investigated the dynamics of the peeling front by following the directional motion of TFAM over a wide range of TFAM concentrations. To accurately assess the effective TFAM concentration on the DNA, we determined the percentage of TFAM coverage of the DNA molecule, which was calculated as described previously (Farge et al., 2012). We analyzed in total 221 fluorescent TFAM patches/spots bound to DNA, on DNA molecules ranging from 1% to 100% TFAM coverage. The obtained velocities of the TFAM molecules were binned according to the percentage of TFAM coverage. The results revealed that, at low TFAM coverage, on average TFAM molecules show a significant velocity (Figure 2E). In contrast, at high TFAM coverage, none of the TFAM molecules display any significant velocity, suggesting that DNA peeling is inhibited. It is interesting to note that, at low TFAM coverage, TFAM molecules exhibit a large range of velocities, with some molecules moving fast and some being stationary (Figure 2E, inset). We explain this result by the coexistence, on the same DNA molecule, of regions undergoing peeling (fast velocity) and regions, which are not yet undergoing peeling or cannot be peeled (stationary).

TFAM binding to nonspecific DNA can induce local base-pair destabilization of DNA (Farge et al., 2012). We thus reasoned that high concentrations of TFAM could stabilize the junctions next to the melting bubbles and, as a consequence, prevent the bubbles from releasing the energy needed for the strand peeling. To exclude this possibility, we decided to consider only the DNA molecules with a low TFAM coverage (<10%) and to investigate the velocities as a function of the number of TFAM molecules in each fluorescent spot. The fluorescence intensity of a single fluorophore was calculated using single photobleaching steps (Figure S1) (Candelli et al., 2013). Our analysis demonstrated that TFAM patches with less than 20 molecules move during peeling, irrespectively of the number of TFAM molecules forming the spots. However, above a threshold of ~20 TFAM per patch, the molecules do not show any significant movements, demonstrating an inhibition of the peeling process by a 20 TFAM filament on the DNA.

TFAM Compaction of DNA Blocks Replication

Our findings so far demonstrated that TFAM filaments block DNA strand separation. This conclusion prompted us to investigate effects on transcription and mtDNA replication, two processes that involve DNA unwinding. We first investigated if a TFAM compacted DNA molecule could be used as template for mitochondrial DNA replication, a process that can be reconstituted in vitro by combining POLγ, the mitochondrial helicase TWINKLE, and mtSSB on a double-stranded DNA template with a preformed replication fork (Korhonen et al., 2004). We used this system to monitor effects of increasing TFAM concentrations (Figure 3A). We observed a slight decrease in mtDNA replication already at TFAM concentrations of 1 TFAM/40–60 bp. The TFAM concentration at this point was about 15–20 nM, well above the previously measured dissociation constant (K_D) for TFAM binding to DNA, which is ~4 nM (Kaufman et al., 2007). When we increased the ratio to 1 TFAM/20 bp, which is similar to the expected in vivo ratio, we noted a decrease in mtDNA replication. A further increase to a ratio of 1 TFAM per 8 bp abolished DNA replication.

We also measured the effects of TFAM levels on DNA binding/compaction (Figure 3B). To this end, we radioactively labeled the DNA template used in the rolling-circle assay and monitored effects of increasing levels of TFAM in an electrophoresis mobility shift assay (EMSA) experiment. At a ratio of 1 TFAM/40 bp, we could not observe nucleoprotein complexes and the template migrated as a naked DNA control (Figure 3B, compare lanes 1 and 2). The formation of a stable nucleoprotein complex was initiated at a ratio of 1 TFAM/20 bp, and full compaction of all DNA was observed when the levels of TFAM were further increased to 1 TFAM/12 bp. Interestingly, this full compaction coincided with a complete blockage of replication (Figure 3C). Our data therefore demonstrated that the DNA replication machinery can function at levels of TFAM similar to those observed in vivo. At higher protein levels, however, TFAM forms a stable nucleoprotein complex with DNA that completely blocks DNA replication.

Finally, we investigated effects of TFAM on the DNA replication machinery in a time course experiment (Figure 3D). Before DNA replication was initiated, we preincubated the template with two different TFAM concentrations. At a lower ratio of TFAM to

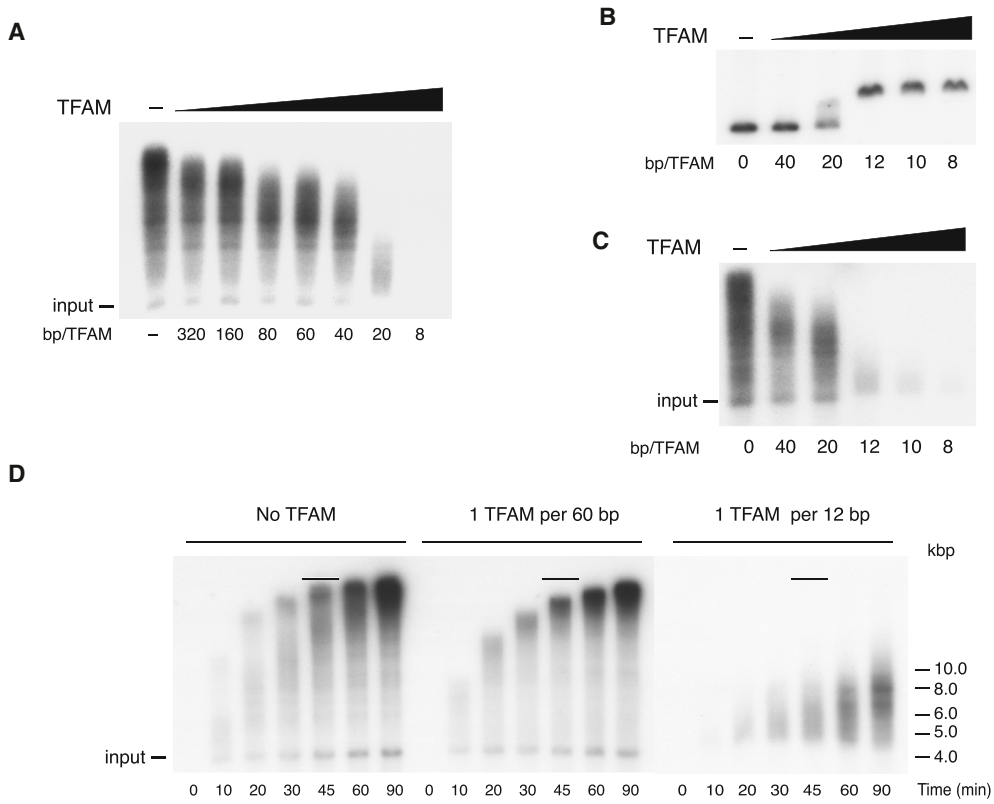

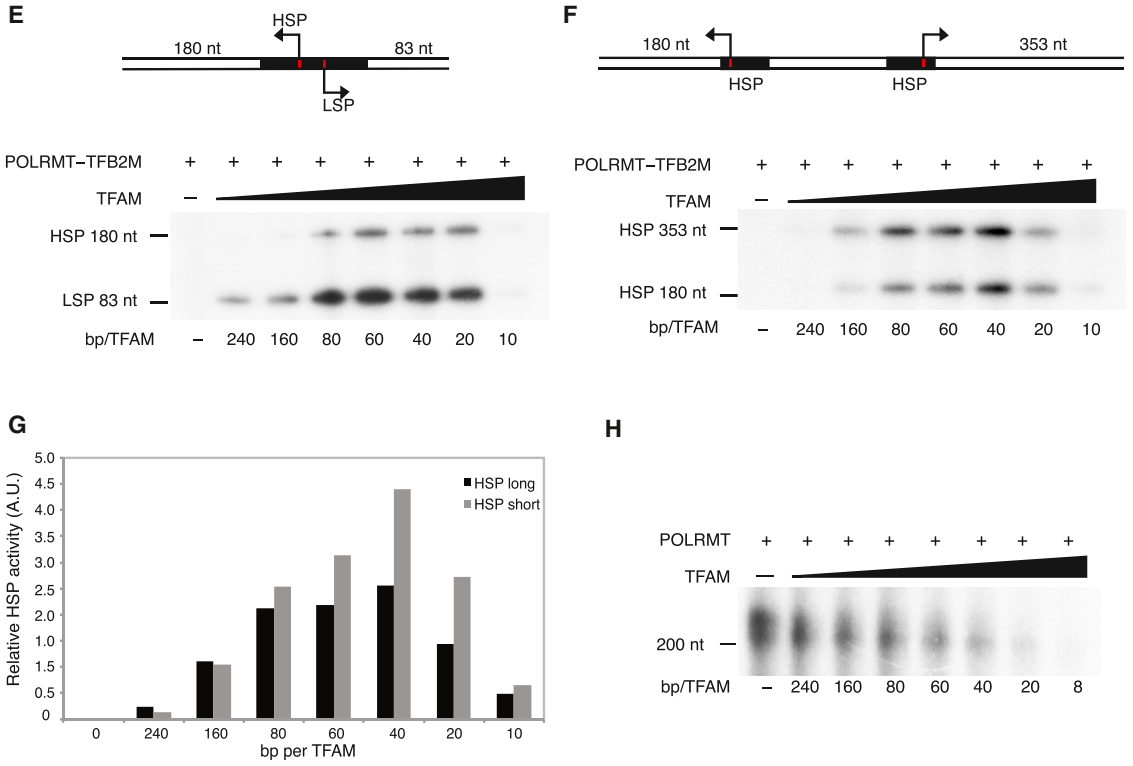

(legend on next page)

DNA (1 TFAM/60 bp), we observed robust levels of DNA synthesis, even if there was a slight delay in the rate of synthesis compared to a naked DNA template. When the TFAM to DNA ratio was increased to 1 TFAM/12 bp, we observed a strong decrease in DNA synthesis. However, the reactions were not completely blocked, since longer products were produced over time. Our experiments therefore demonstrated that DNA replication can progress also at higher TFAM ratios, but at a substantially reduced rate.

TFAM Compaction of DNA Blocks Transcription

Next, we monitored if TFAM compaction also affected transcription, using a reconstituted in vitro transcription system containing TFAM, POLRMT, and TFB2M (Falkenberg et al., 2002). We first used the natural HSP1/LSP cassette cloned from mtDNA, in which the two divergent transcription start sites are separated by only 160 nt (Figure 3E). We noted a dramatic drop in transcription when TFAM ratios were increased above the estimated in vivo rates of 1 TFAM per ~15–18 bp of mtDNA (Figure 3E, compare the two rightmost lanes). We wondered if the inhibitory effect of TFAM involved blockage of the transcription elongation step, which requires unwinding of duplex DNA. The HSP1/LSP construct could not be used to address this question, since the two promoters differ in their TFAM dependence. To address the question, we instead used a linearized plasmid DNA template with two divergent transcription units under the control of identical promoters (HSP1) but generating different length transcripts (180 nt and 353 nt). We could now investigate if the longer transcription unit was more sensitive to TFAM levels than the shorter unit, which would be the expected outcome if TFAM affects the elongation step (Figure 3F). Transcription initiation required a ratio of 1 TFAM/160 bp, and optimal activity was reached at a ratio of 1 TFAM/40 bp (corresponding 260 nM TFAM). A further increase in the TFAM to DNA ratio caused a sharp decrease in transcription, and the effect paralleled that observed for DNA replication (see above). When we monitored the relative levels of short and long transcripts, adjusting for the number of incorporated α^{32}-P-UTP, we observed that the longer, 353 nt transcript was more affected by higher TFAM concentrations than the shorter, 180 nt transcript (Figure 3G). The observation that the long transcription unit was more sensitive to high TFAM concentrations than the shorter transcription unit indicated that TFAM impairs transcription elongation.

To further demonstrate that the observed negative effects of TFAM were due to inhibition of transcription elongation, we used a tailed template assay. POLRMT can initiate transcription on duplex DNA that has a short, single-stranded 3′ tail, making this an ideal assay to monitor effects on transcription elongation independent of promoter recognition (Falkenberg et al., 2002). Our experiments demonstrated that POLRMT alone could initiate transcription on a tailed template and that increasing levels of TFAM blocked this reaction (Figure 3H).

Compacted and Nearly Naked DNA Molecules Coexist at Physiological TFAM Concentrations

To directly visualize the consequences of increasing TFAM levels for mtDNA packaging, we used atomic force microscopy (AFM). We incubated linearized DNA molecules with increasing concentrations of TFAM and recorded images of the formed nucleoprotein complexes. Linear DNA molecules were readily observed (Figure 4A), and at a lower TFAM ratio (1 TFAM/40 bp DNA), we could only observe a few bound TFAM molecules (Figure 4B). If we increased the TFAM concentration further, to levels similar to those observed in vivo (1 TFAM per 20 bp DNA), we observed different degrees of compaction, ranging from almost naked DNA to fully compacted nucleoprotein complexes (Figure 4C). The coexistence of free DNA and highly compacted nucleoprotein complexes supports the idea that TFAM binds with high positive cooperativity to DNA (Figure S2). This is consistent with our previous work where we systematically investigated cooperative DNA binding of TFAM (Farge et al., 2012). A further increase of TFAM concentrations to 1 TFAM/10 bp DNA caused nearly all DNA molecules to form compact nucleoprotein complexes (Figure 4D). From the AFM images, we determined the contour length of the noncompacted parts of DNA (Figure 4E; Supplemental Experimental Procedures). TFAM packaging of DNA caused a dramatic decrease in the "contour length" of DNA, from ~1.4 μm for naked DNA to less than 0.1 μm for completely covered DNA, demonstrating the ability of TFAM to package DNA into compact, spherical nucleoprotein structures. We noticed that the maximum contour length we measured never exceeded the expected contour length of the DNA template, making very unlikely the presence of multiple DNA molecules entangled. We also sometimes observed some material scattered around the DNA that we interpreted as TFAM that has dissociated from the DNA after deposition. Our experiments

Figure 3. TFAM Packaging Inhibits mtDNA Replication and Transcription

(A) Rolling-circle DNA replication performed in the presence of radioactive [α-32P] dCTP. Increasing TFAM:DNA ratios leads to an inhibition of replication.

(B) Electrophoresis mobility shift assay (EMSA) using a radioactively labeled ([γ-ATP]^{32}P) rolling-circle template in the presence of increasing TFAM concentrations. The TFAM:DNA ratios are indicated.

(C) Rolling-circle DNA replication using the same TFAM:DNA ratios as in (B).

(D) DNA replication as a function of time in the presence of: no TFAM, 1 TFAM/60 bp, or 1 TFAM/12 bp. The bar is present on the same level in all three experiments.

(E) In vitro transcription reactions were performed in the presence of POLRMT (640 fmol), TFB2M (1.2 pmol), and increasing ratios of TFAM to DNA, as indicated. An mtDNA fragment containing the divergent HSP1 and LSP promoters was used as template.

(F) In vitro transcription reactions were performed as in (A). The linearized template contained two HSP1 promoters, generating products of 180 and 353 nt, respectively.

(G) Phosphoimaging was used to quantify the relative effects of increasing TFAM:DNA ratios on the long and short transcript generated in the experiment depicted in (F).

(H) Promoter-independent transcription was monitored using a DNA template with a free 3′ tail. The reactions were performed in the presence of POLRMT (2.5 pmol) and increasing ratios of TFAM to DNA, as indicated.

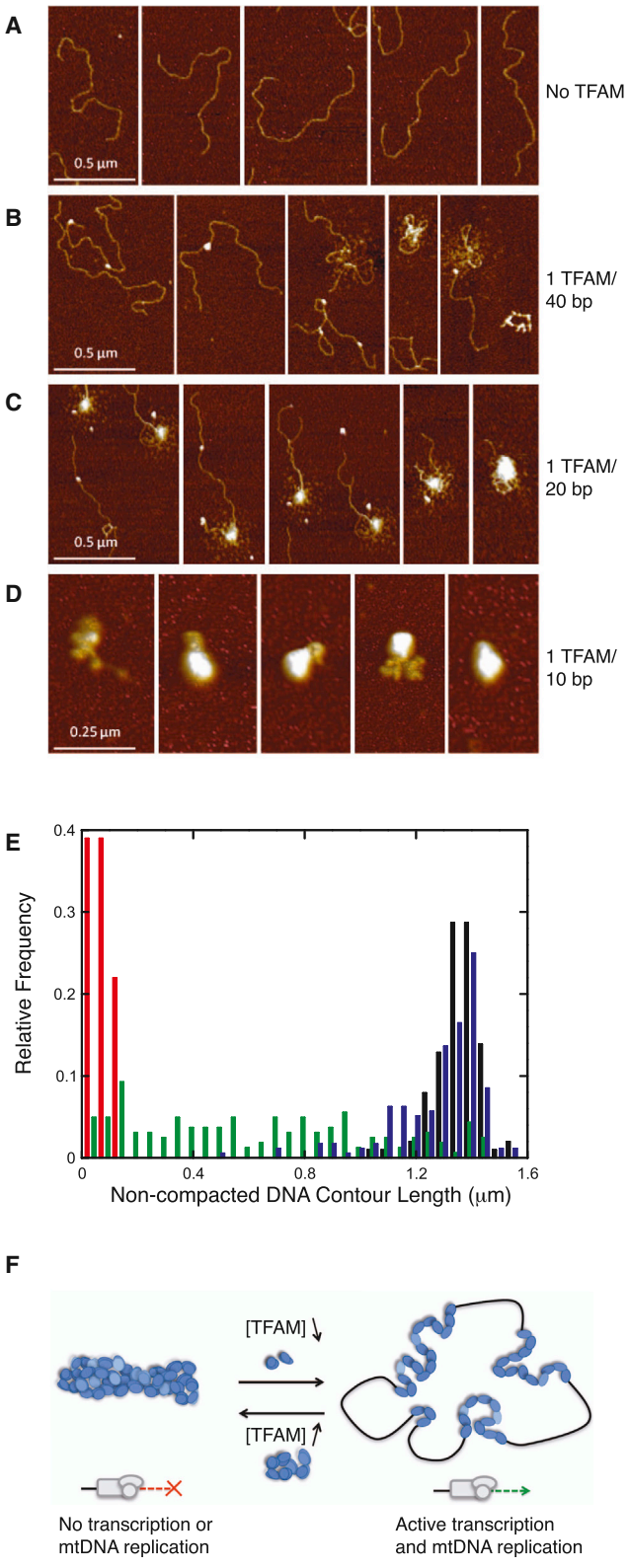

Figure 4. Distribution of DNA Compaction at Different TFAM Concentrations

(A–D) Atomic force microscopy images of TFAM-DNA complexes at increasing TFAM concentrations: (A) naked DNA, (B) 40 bp per TFAM molecule, (C) 20 bp per TFAM molecule, and (D) 10 bp per TFAM molecule.

(E) Histogram of the measured DNA contour length at different TFAM concentrations: naked DNA (black), 40 bp per TFAM molecule (blue), 20 bp per TFAM molecule (green), and 10 bp per TFAM molecule (red). The visible contour length, reflecting the level of compaction, was determined as described in Experimental Procedures. DNA length = 4,348 bp (~1.4 μm).

(F) Variations in TFAM concentrations influence the fraction of active nucleoids in vitro. TFAM is depicted in blue, and the transcription and DNA replication machineries are in gray. Please see Campbell et al. (2012) for comparison. See also Figure S2.

demonstrated that small changes in the TFAM:mtDNA ratio had dramatic consequences for mtDNA packaging and that at TFAM concentrations close to those observed in vivo, both compacted and nearly completely naked DNA molecules could be observed.

DISCUSSION

TFAM binds DNA with positive cooperativity, and we here demonstrate that small changes in TFAM concentrations can have dramatic consequences for the number of mtDNA molecules available for enzymatic activities where DNA unwinding is required, i.e., transcription and DNA replication (Figure 4F). In the nucleus, there are only two copies available of each gene. Because of this, the cell has developed a highly complex system for gene regulation, with gene-specific transcription factors that may stimulate the frequency of transcription a 1,000-fold or more. In contrast, the mitochondrial genome is present in 1,000–10,000 copies in a somatic cell. This large number means that gene transcription can be regulated not only by changing the frequency of transcription of a specific mtDNA molecule but also by regulating the fraction of mtDNA molecules used for active transcription. The ability to regulate the fraction of active mtDNA molecules may also be of relevance during mtDNA replication. A pathogenic mtDNA mutation can be present in all copies (homoplasmy) or only in a fraction of all copies (heteroplasmy) in a mammalian cell. The levels of mtDNA heteroplasmy differ between mother and offspring, demonstrating the existence of a genetic bottleneck, which depends on the replication of a subset of mtDNA molecules within the developing maternal germline (Falkenberg et al., 2007; Freyer et al., 2012). Therefore, there could be mechanisms that select only a subset of mtDNA molecules for replication, whereas others remain in a silent state.

We demonstrate here that TFAM packaging can silence DNA and that the protein may regulate the fraction of mitochondrial genomes available for DNA transactions. Our data suggest that it is important to maintain the ratio of TFAM to mtDNA within a narrow range, since small variations may have dramatic functional effects for transcription and mtDNA replication. In agreement with this idea, a mild increase in TFAM levels in vivo (~2-fold) leads to a proportional increase in mtDNA copy number (Ekstrand et al., 2004). Furthermore, forced overexpression of TFAM results in mtDNA depletion in HEK293 cell lines (Pohjoismäki et al., 2006). In this later case, the compensatory mechanisms (i.e., increased mtDNA replication) may not be sufficiently

efficient to keep up with the increased TFAM levels. This leads to a change in the TFAM to mtDNA ratio, which in turn closes down mtDNA, impairs mtDNA replication, and causes mtDNA depletion.

TFAM levels are regulated in vivo by the Lon protease (Matsushima et al., 2010). Depletion of Lon leads to an increase in TFAM levels and mtDNA copy number. Conversely, overexpression of Lon leads to reduction of TFAM and a decrease in mtDNA copy number. Interestingly, when cells were cultured in the presence of ethidium bromide, which causes mtDNA depletion, Lon knockdown cells are unable to degrade TFAM, which in turn leads to a strong increase in the TFAM:mtDNA ratio (Matsushima et al., 2010). This change in the TFAM:mtDNA ratio causes an inhibition of mitochondrial transcription. This finding is thus in excellent agreement with results presented in this report and provides in vivo support for our proposed model, in which an increased ratio of TFAM to DNA inhibits DNA melting and thus blocks active transcription.

EXPERIMENTAL PROCEDURES

Detailed experimental procedures are provided in Supplemental Experimental Procedures.

Protein Preparation and Labeling

TFAM, TFB2M, POLRMT, TWINKLE, POLγ, and mtSSB were purified in recombinant form. For fluorescent labeling of mouse TFAM, we introduced an additional cysteine residue in the C-terminal end, which was labeled with maleimide Alexa-555 dye (Molecular Probes) as described in Supplemental Experimental Procedures.

In Vitro Analysis of DNA Replication and Transcription

DNA replication reactions were carried out using a dsDNA template with a preformed replication fork in the presence of TWINKLE, POLγ, and mtSSB as described in Supplemental Experimental Procedures. TFAM was added as indicated in the figures and the concentrations are given as TFAM molecules per bp of template DNA (see details in Supplemental Experimental Procedures). The time-course experiment was performed in a total reaction volume of 150 μl, and at the times indicated, 25 μl was removed and analyzed. For EMSA experiments, we used the same template as in our rolling-circle DNA replication experiments that had been radioactively labeled with [γ-^{32}P]ATP at the 5′ end of the single-stranded tail. The labeled template (5 fmol) was incubated with the indicated concentrations of TFAM for 10 min on ice before analysis on a 0.8% native agarose gel. In vitro transcription reactions contained POLRMT, TFB2M, the indicated ratio of TFAM to DNA, and a final concentration of 80 mM NaCl. The reactions were terminated after 30 min and analyzed as previously described (Shi et al., 2012). The 200 bp tailed template was designed to have a 15 nt single-stranded tail at the 3′ end.

DNA Substrate for Optical Tweezers

The 3′ and 5′ ends of lambda DNA (Roche) were labeled with biotin as described previously (Candelli et al., 2013).

Optical Trapping, Fluorescence Microscopy, and Atomic Force Microscopy

The combined single-molecule fluorescence and optical trapping instrument and the custom-built microfluidic flow system with multiple laminar channels have been described in detail elsewhere (Gross et al., 2010). Before use, the flow cell was coated with casein (100 μg/ml) in order to decrease the adsorption of the protein to the glass surface. The acquired movies were analyzed with a custom-written tracking program (LabVIEW). The linearized DNA used for AFM was a modified version of pBluescript plasmid in which an unspecific DNA fragment of 1,384 bp was introduced at the EcoRI site (pBS-LSPH, 4,348 bp). Samples were directly imaged in an AFM (Bruker BioCatalyst System, Peak Force Tapping mode at 1.5 kHz) using a SiN cantilever (Olympus OMCL-RC800PSA, k = 0.8 N/m). The contour length was determined as described in Supplemental Experimental Procedures.

SUPPLEMENTAL INFORMATION

Supplemental Information includes Supplemental Experimental Procedures, two figures, and one movie and can be found with this article online at http://dx.doi.org/10.1016/j.celrep.2014.05.046.

AUTHOR CONTRIBUTIONS

G.F., M.M., M.B., S.M.J.L.v.d.W., C.M.G., G.J.L.W., and M.F. conceived and designed the experiments. G.F., M.M., M.B., S.M.J.L.v.d.W., and M.F. performed the experiments. G.F., M.M., M.B., S.M.J.L.v.d.W., W.H.R., G.J.L.W., and M.F. analyzed the data. G.F., M.M., S.M.J.L.v.d.W., C.M.G., G.J.L.W., and M.F. wrote the paper.

ACKNOWLEDGMENTS

The authors would like to thank Bram Mooij for his help with collecting data, Graeme King for his advice on RPA use, and Mauro Modesti for providing the fluorescently labeled RPA. This study was supported by Swedish Research Council grants (to M.F. and C.M.G.), the Swedish Cancer Foundation (to M.F. and C.M.G.), the Wallenberg foundation (to M.F. and C.M.G.), an ERC Advanced Investigator grant (to C.M.G.), and an ERC Starting Independent Investigator grant (to M.F. and G.J.L.W.). Finally, we acknowledge the support by a NWO VICI grant (to G.J.L.W.) and a VIDI grant (to W.H.R.).

Received: October 14, 2013
Revised: April 11, 2014
Accepted: May 27, 2014
Published: June 26, 2014

REFERENCES

Bogenhagen, D.F. (2012). Mitochondrial DNA nucleoid structure. Biochim. Biophys. Acta *1819*, 914–920.

Brown, T.A., Tkachuk, A.N., Shtengel, G., Kopek, B.G., Bogenhagen, D.F., Hess, H.F., and Clayton, D.A. (2011). Superresolution fluorescence imaging of mitochondrial nucleoids reveals their spatial range, limits, and membrane interaction. Mol. Cell. Biol. *31*, 4994–5010.

Campbell, C.T., Kolesar, J.E., and Kaufman, B.A. (2012). Mitochondrial transcription factor A regulates mitochondrial transcription initiation, DNA packaging, and genome copy number. Biochim. Biophys. Acta *1819*, 921–929.

Candelli, A., Hoekstra, T.P., Farge, G., Gross, P., Peterman, E.J., and Wuite, G.J. (2013). A toolbox for generating single-stranded DNA in optical tweezers experiments. Biopolymers *99*, 611–620.

Ekstrand, M.I., Falkenberg, M., Rantanen, A., Park, C.B., Gaspari, M., Hultenby, K., Rustin, P., Gustafsson, C.M., and Larsson, N.G. (2004). Mitochondrial transcription factor A regulates mtDNA copy number in mammals. Hum. Mol. Genet. *13*, 935–944.

Falkenberg, M., Gaspari, M., Rantanen, A., Trifunovic, A., Larsson, N.G., and Gustafsson, C.M. (2002). Mitochondrial transcription factors B1 and B2 activate transcription of human mtDNA. Nat. Genet. *31*, 289–294.

Falkenberg, M., Larsson, N.G., and Gustafsson, C.M. (2007). DNA replication and transcription in mammalian mitochondria. Annu. Rev. Biochem. *76*, 679–699.

Farge, G., Laurens, N., Broekmans, O.D., van den Wildenberg, S.M., Dekker, L.C., Gaspari, M., Gustafsson, C.M., Peterman, E.J., Falkenberg, M., and Wuite, G.J. (2012). Protein sliding and DNA denaturation are essential for DNA organization by human mitochondrial transcription factor A. Nat. Commun. *3*, 1013.

Finkelstein, I.J., and Greene, E.C. (2013). Molecular traffic jams on DNA. Annu. Rev. Biophys. *42*, 241–263.

Fisher, R.P., and Clayton, D.A. (1985). A transcription factor required for promoter recognition by human mitochondrial RNA polymerase. Accurate initiation at the heavy- and light-strand promoters dissected and reconstituted in vitro. J. Biol. Chem. *260*, 11330–11338.

Freyer, C., Cree, L.M., Mourier, A., Stewart, J.B., Koolmeister, C., Milenkovic, D., Wai, T., Floros, V.I., Hagström, E., Chatzidaki, E.E., et al. (2012). Variation in germline mtDNA heteroplasmy is determined prenatally but modified during subsequent transmission. Nat. Genet. *44*, 1282–1285.

Gross, P., Farge, G., Peterman, E.J., and Wuite, G.J. (2010). Combining optical tweezers, single-molecule fluorescence microscopy, and microfluidics for studies of DNA-protein interactions. Methods Enzymol. *475*, 427–453.

Kanki, T., Ohgaki, K., Gaspari, M., Gustafsson, C.M., Fukuoh, A., Sasaki, N., Hamasaki, N., and Kang, D. (2004). Architectural role of mitochondrial transcription factor A in maintenance of human mitochondrial DNA. Mol. Cell. Biol. *24*, 9823–9834.

Kaufman, B.A., Durisic, N., Mativetsky, J.M., Costantino, S., Hancock, M.A., Grutter, P., and Shoubridge, E.A. (2007). The mitochondrial transcription factor TFAM coordinates the assembly of multiple DNA molecules into nucleoid-like structures. Mol. Biol. Cell *18*, 3225–3236.

King, G.A., Gross, P., Bockelmann, U., Modesti, M., Wuite, G.J., and Peterman, E.J. (2013). Revealing the competition between peeled ssDNA, melting bubbles, and S-DNA during DNA overstretching using fluorescence microscopy. Proc. Natl. Acad. Sci. USA *110*, 3859–3864.

Korhonen, J.A., Pham, X.H., Pellegrini, M., and Falkenberg, M. (2004). Reconstitution of a minimal mtDNA replisome in vitro. EMBO J. *23*, 2423–2429.

Kukat, C., and Larsson, N.G. (2013). mtDNA makes a U-turn for the mitochondrial nucleoid. Trends Cell Biol. *23*, 457–463.

Kukat, C., Wurm, C.A., Spåhr, H., Falkenberg, M., Larsson, N.G., and Jakobs, S. (2011). Super-resolution microscopy reveals that mammalian mitochondrial nucleoids have a uniform size and frequently contain a single copy of mtDNA. Proc. Natl. Acad. Sci. USA *108*, 13534–13539.

Larsson, N.G., Wang, J., Wilhelmsson, H., Oldfors, A., Rustin, P., Lewandoski, M., Barsh, G.S., and Clayton, D.A. (1998). Mitochondrial transcription factor A is necessary for mtDNA maintenance and embryogenesis in mice. Nat. Genet. *18*, 231–236.

Matsushima, Y., Goto, Y., and Kaguni, L.S. (2010). Mitochondrial Lon protease regulates mitochondrial DNA copy number and transcription by selective degradation of mitochondrial transcription factor A (TFAM). Proc. Natl. Acad. Sci. USA *107*, 18410–18415.

Ngo, H.B., Kaiser, J.T., and Chan, D.C. (2011). The mitochondrial transcription and packaging factor Tfam imposes a U-turn on mitochondrial DNA. Nat. Struct. Mol. Biol. *18*, 1290–1296.

Park, C.B., and Larsson, N.G. (2011). Mitochondrial DNA mutations in disease and aging. J. Cell Biol. *193*, 809–818.

Pohjoismäki, J.L., Wanrooij, S., Hyvärinen, A.K., Goffart, S., Holt, I.J., Spelbrink, J.N., and Jacobs, H.T. (2006). Alterations to the expression level of mitochondrial transcription factor A, TFAM, modify the mode of mitochondrial DNA replication in cultured human cells. Nucleic Acids Res. *34*, 5815–5828.

Rubio-Cosials, A., Sidow, J.F., Jiménez-Menéndez, N., Fernández-Millán, P., Montoya, J., Jacobs, H.T., Coll, M., Bernadó, P., and Solà, M. (2011). Human mitochondrial transcription factor A induces a U-turn structure in the light strand promoter. Nat. Struct. Mol. Biol. *18*, 1281–1289.

Shi, Y., Dierckx, A., Wanrooij, P.H., Wanrooij, S., Larsson, N.G., Wilhelmsson, L.M., Falkenberg, M., and Gustafsson, C.M. (2012). Mammalian transcription factor A is a core component of the mitochondrial transcription machinery. Proc. Natl. Acad. Sci. USA *109*, 16510–16515.

van Mameren, J., Gross, P., Farge, G., Hooijman, P., Modesti, M., Falkenberg, M., Wuite, G.J., and Peterman, E.J. (2009). Unraveling the structure of DNA during overstretching by using multicolor, single-molecule fluorescence imaging. Proc. Natl. Acad. Sci. USA *106*, 18231–18236.

Wang, Y.E., Marinov, G.K., Wold, B.J., and Chan, D.C. (2013). Genome-wide analysis reveals coating of the mitochondrial genome by TFAM. PLoS ONE *8*, e74513.